INTEGRATING MECHANOBIOLOGY AND BIOMECHANICS TO CHARACTERIZE MICROVASCULAR ADAPTATION TO PULSATILE BLOOD FLOW

An Undergraduate Research Scholars Thesis

by

SARA AHMED & TIA BIMAL

Submitted to Honors and Undergraduate Research
Texas A&M University
in partial fulfillment of the requirements for the designation as

UNDERGRADUATE RESEARCH SCHOLAR

Approved by
Research Advisor: Dr. Christopher M. Quick

May 2014

Majors: Biomedical Engineering
Biomedical Sciences

TABLE OF CONTENTS

PAGE

ABSTRACT 1

DEDICATION 3

ACKNOWLEDGEMENTS 4

CHAPTER

I INTRODUCTION 5

II METHODS 8

Modeling Blood Flow in the Vessels 8
Creating the Network of Capillaries 9
Preparing Input Blood Flow 10
Characterizing the Shear Stress 10
The Adaptive Response to Mechanical Stress 11

III RESULTS 12

IV DISCUSSION 21

V CONCLUSION 23

REFERENCES 25

APPENDIX A 28

APPENDIX B 30

APPENDIX C 33

APPENDIX D 35

APPENDIX E 37

APPENDIX F 44

APPENDIX G 45

CONTACTS 46

ABSTRACT

Integrating Mechanobiology and Biomechanics to Characterize Microvascular Adaptation to Pulsatile Blood Flow. (May 2014)

Sara Ahmed
Department of Biomedical Engineering

Tia Bimal
Department of Biomedical Sciences
Texas A&M University

Research Advisor: Dr. Christopher Quick
Department of Veterinary Physiology and Pharmacology

Continuous-flow left-ventricular assist device (LVAD) implantation leads to increased peripheral resistance and development of arteriovenous malformations. These comorbidities have resisted mechanistic explanation, in part because normal microvascular adaptation has not yet been fully characterized. In fact, standard mathematical models using the common assumption that vessels solely adapt to steady flow do not reproduce normal vascular structure. Therefore, we developed a simple, mathematical model of a branching microvascular network to test the hypothesis that pulsatile blood flow is necessary for microvascular stability. First, we assumed a microvascular network with a simple branching pattern and vessel properties like those measured *in situ*. Second, we predicted pulsatile shear stresses using the standard transmission-line equations, which are typically used to characterize pulse transmission in large conductance arteries. Third, we assumed vessel radii increase in response to increasing pulsatile endothelial shear stress. Evaluating the model iteratively to simulate the adaptive process yielded a stable network with normal radii. Decreasing pulsatility of the inlet blood flow caused decreases in vessel radii and the manifestation of capillary rarefaction, both of which increase microvascular resistance. In

extreme cases, reduced pulsatility leads to an absence of capillaries and the formation of arteriovenous malformations. Identifying the fundamental cause of the devastating complications of LVAD implantation arose from integrating the typically isolated fields of biomechanics and mechanobiology, allowing the translation of basic research at the level of a single vessel to clinically-relevant research at a systemic level.

DEDICATION

We would like to dedicate our thesis to Dr. Waqar Mohiuddin. Your tutelage helped make the research process less intimidating and more manageable when we first dove into it. We are deeply indebted to you, and wish you every success in your new position.

ACKNOWLEDGEMENTS

We are immensely grateful to Phuc Nyguen and Dr. Christopher Quick for their tremendous support without which this project would not have been conceived, let alone have been successful. Their guidance and patience were paramount to the accomplishment of this thesis. Phuc was studying adaptation in larger arterial vessels and was generous enough to let us use his adaptive functions as a springboard for our microvascular adaptation project.

Also of note were the contributions made by Alexis Luedke, Lauren Dale, Steven Haas, and Felipe Flores. Their work ethic and dedication held steady throughout the semester, but really shone through when the going got tough. Steven especially was tireless in his pursuit of resolving the fundamental question we proposed to solve.

Lastly, we would like to thank the Honors and Undergraduate Research Office at Texas A&M University for giving us the unparalleled opportunity to publish our thesis. Their ongoing communication and advice were of great help, and we truly appreciate all of their input.

CHAPTER I

INTRODUCTION

Heart failure is a serious medical condition impacting an estimated 5.1 million Americans over twenty years of age [1]. Implantation of a ventricular assist device (VAD) is indicated for those suffering from irreversible ventricular failure. Though originally developed as a bridge to transplantation, VADs have also become popular as a destination therapy for patients who are not candidates for a heart transplant [2]. While VAD implantation serves to significantly increase both patient life span and quality of life, it also gives rise to a myriad of complications, including capillary rarefaction and arteriovenous malformations [3]. As many as 33% of VAD recipients experience internal bleeding in the intestinal, genitourinary, intracranial, or other remote organ systems [4].

The VAD is a mechanical device that aids in blood propulsion. As previously mentioned, VADs are typically used in patients who's failing hearts are not strong enough to pump blood through the circulatory system [5]. As shown in *Figure 1*, the VAD consist of two tubes and a pump. The first tube connects a ventricle of the heart to a pump. This pump propels blood through the second tube and into the aorta from which the blood is carried to the rest of the body. The VAD also has a control unit that monitors the function of the device and alerts the patient when its power is low or if the device is experiencing an error. The most durable and commonly used type of VAD is the continuous-flow pump [6]. Continuous-flow VADs (CF-VAD) use an axial flow pump that propels blood at a nearly constant rate.

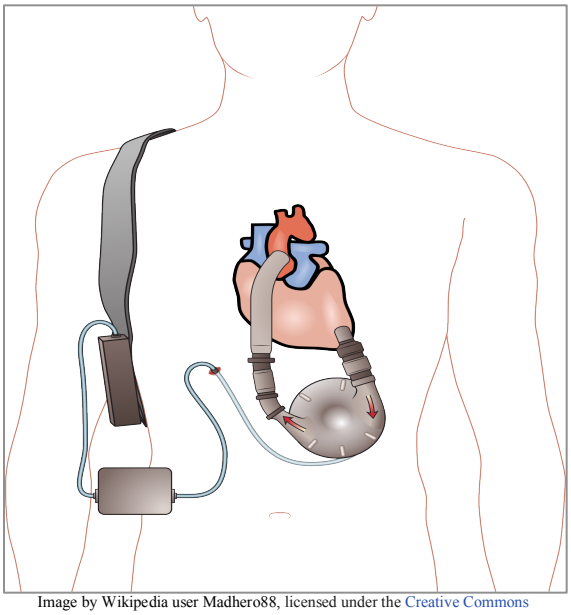

Figure 1. *The Continuous Flow Left Ventricular Assist Device (CF-LVAD). The CF-LVAD pumps blood from the left ventricle to the pump that propels the blood through the aorta to the rest of the body. CF-LVAD is externally connected to a battery pack and a control unit.*

Because most VADs on the market today pump blood at a constant rate, it can reduce pulsatility or even render the patient effectively "pulseless' [5]. Under normal conditions, the heart generates a significant pulse of blood with each beat [7]. This pulse is then transmitted through the vessels of the cardiovascular system all the way down to the capillaries, as shown in *Figure 2* [8]. Blood pressure pulses generated by the heart are "sensed" by the endothelial cells in the walls of the arterial vessels [9]. As the vessels branch and become smaller, the pulses are first increased, before being attenuated as they enter the microvasculature [10,11]. Thus it is possible to conclude that while VAD implantation increases the overall amount of blood flow, it diminishes the pulsatility of that flow.

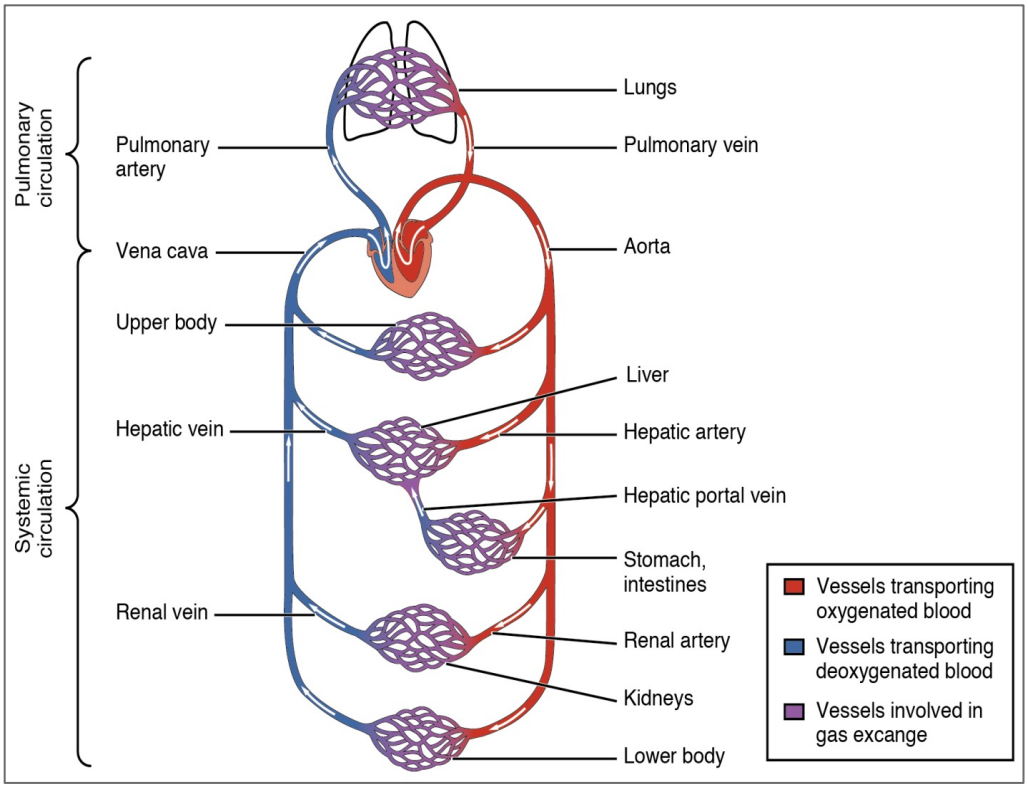

Figure 2. *The Path of Blood Flow through the Circulatory System. This is a simplified image that shows the path of blood flow through systemic and pulmonary circulation.*

Unfortunately, VADs are not unique in their production of this phenomenon. Aortic coarctations and atherosclerotic plaques have been observed to cause both similar reductions in pulsatility and similar adverse effects [12]. Therefore, the purpose of the present work is to use a mathematical model to test the hypothesis that pulsatile endothelial shear stress is a critical mechanical stimulus that prevents capillary rarefaction and AVM development.

CHAPTER II

METHODS

Modeling Blood Flow in the Vessels

Because blood is an incompressible fluid, its flow is characterized by the Navier-Stokes equation. We simplified this statement of conservation of linear momentum for one dimension, as is common when describing pulsatile hemodynamics [13,14]. This approach assumes that entrance phenomena, rotational flow, radial flow, and body forces are negligible. Because of this, only arterial compliance, viscosity, and inertial effects due to the mass of the blood are left to be characterized. In addition, assuming vessel segment lengths are small, it is possible to further simplify the Navier-Stokes equation into a first-order ordinary differential equation. This final form of the equation relates the pressure (P) to the flow (Q), resistance (R), and inertance (L) per unit length along the blood vessel,

$$-\frac{dP}{dz} = RQ + L\frac{dQ}{dt}, \tag{1}$$

in which z is the axial position along the length of the vessel and t the time. Further, conservation of mass must be considered. Because of this, the amount of blood stored in a compliant artery at any point in time (due to a change in the pressure) causes a corresponding decrease in the flow rate along the vessel's axial position,

$$-\frac{dQ}{dz} = C\frac{dP}{dt}, \tag{2}$$

in which C is the compliance per unit length. The compliance of the vessel is defined as the ratio of changes in the cross-sectional area with respect to changes in the distending pressure. It is possible to assuming that the blood is modeled as a Newtonian fluid and that the arteries are

linearly elastic. From this, the parameters L, C, and R may be computed from the known characteristics and properties of the blood, combined with the structural and mechanical variables of blood vessels.

$$R = \frac{8\mu}{\pi r^4} \quad (3a)$$

$$L = \frac{\rho}{\pi r^2} \quad (3b)$$

$$C = \frac{3\pi r^2 (r+h)^2}{Eh(2r+h)} \quad (3c)$$

in which r is the luminal radius, h is the wall thickness, and E is Young's modulus of the vessel walls. In addition, μ is the dynamic viscosity of blood, and ρ is the density of blood.

Creating the Network of Capillaries

A simple model of the microvascular structure was created by delineating a branching network of 7 vessels, as shown below in *Figure 3*. The properties of the vessels themselves (length, Young's modulus, and initial radii) were taken from measured normal physiological values described by Salotto et al. and Smaje et al. This was a sufficient number of vessels to accurately model the bifurcating nature of the microvessels, without compromising clarity. This model allowed us to characterize the change in flow in response to the changing pulsatile shear stress.

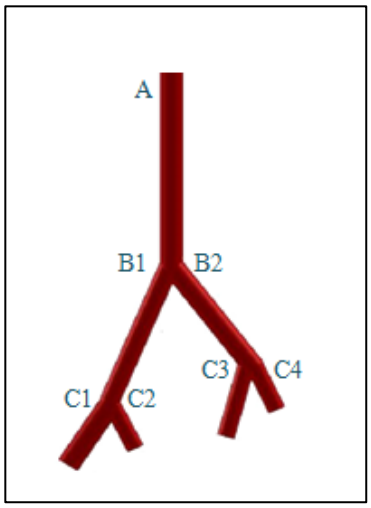

Figure 3. *A Seven-Branch Microvascular Network. A simple network of microvessels in which the radii range from 100 to 27 microns allowed us to study the adaptation of vessels to a pulsatile shear stress.*

Preparing Input Blood Flow

Initially, blood flow from the heart was assumed. We then used the Fourier representation from a previous study to reconstruct this [13]. The flow wave was then scaled down in accordance with the model's location in the capillary bed. As previously described by Nguyen et al., we adjusted our waveform to be comparable to the blood flow in a healthy adult with a measured systolic pressure of 120 mmHg, diastolic pressure of 80 mmHg, and heart rate of 72 beats per minute.

Characterizing the Shear Stress

In conducting arteries, blood pressures and flows at each location vary significantly with time throughout the cardiac cycle. The attending shear stress on the endothelial lining of the vessels (τ) is thus also time-dependent. The shear stress acting on the endothelium in the axial direction may be directly calculated from the time-dependent axial pressure gradient ΔP.

$$\tau(t) = \frac{r}{l} \cdot \Delta P(t) \qquad (4)$$

The time-dependent endothelial shear stress is also averaged in the axial direction over the vessel length. In order to fully characterize the effects of both the altered mean and the altered pulsatile values of shear stress, we used the root mean squared (RMS) values of the mechanical stimulus (τ_{rms}) over a cardiac cycle with a period *T* instead of the instantaneous time-dependent values.

$$\tau_{rms} = \sqrt{\frac{1}{T}\int_0^T \tau(t)^2\, dt} \qquad (5)$$

The RMS value represents an effective value that changes with both the mean (steady) and pulsatile values of the stress.

The Adaptive Response to Mechanical Stress

Chronic adaptation of blood vessels was modeled as first described by Nguyen et al., but our work focuses on how the radius adapts to pulsatile shear stress, rather than how the wall thickness and modulus adapt. Thus an adaptive rule can be identified to model the interactions between this structural variable and the mechanical stimulus.

$$r = r_o + \alpha_\tau \cdot \tau_{rms} \qquad (6)$$

The parameters describing adaptation (r_o, α_τ) characterize the adaptive process and must be empirically determined.

For all simulations, the initial values of *r* for all vessels are assumed to be 1 mm. The iterative process to determine equilibrium structure may be summarized as follows: 1) calculate pulsatile pressures and flows in all vessels using the microvascular network model, 2) calculate the associated τ_{rms} (Eq. 5), and 3) calculate the adapted values for *r* (Eq. 6). Steady state is assumed when the average error between the current values and previous values of *r* is less than 0.001%.

CHAPTER III

RESULTS

A reduction in inlet pulsatile blood flow resulted in decreased microvascular radii. A decreased vascular radii in turn caused an increase in resistance to blood flow (*Figure 4a*). As pressure and resistance are directly proportional, a decrease in pulsatile shear stress resulted in an increase in pulsatile pressure within the microvessels (*Figure 4b*).

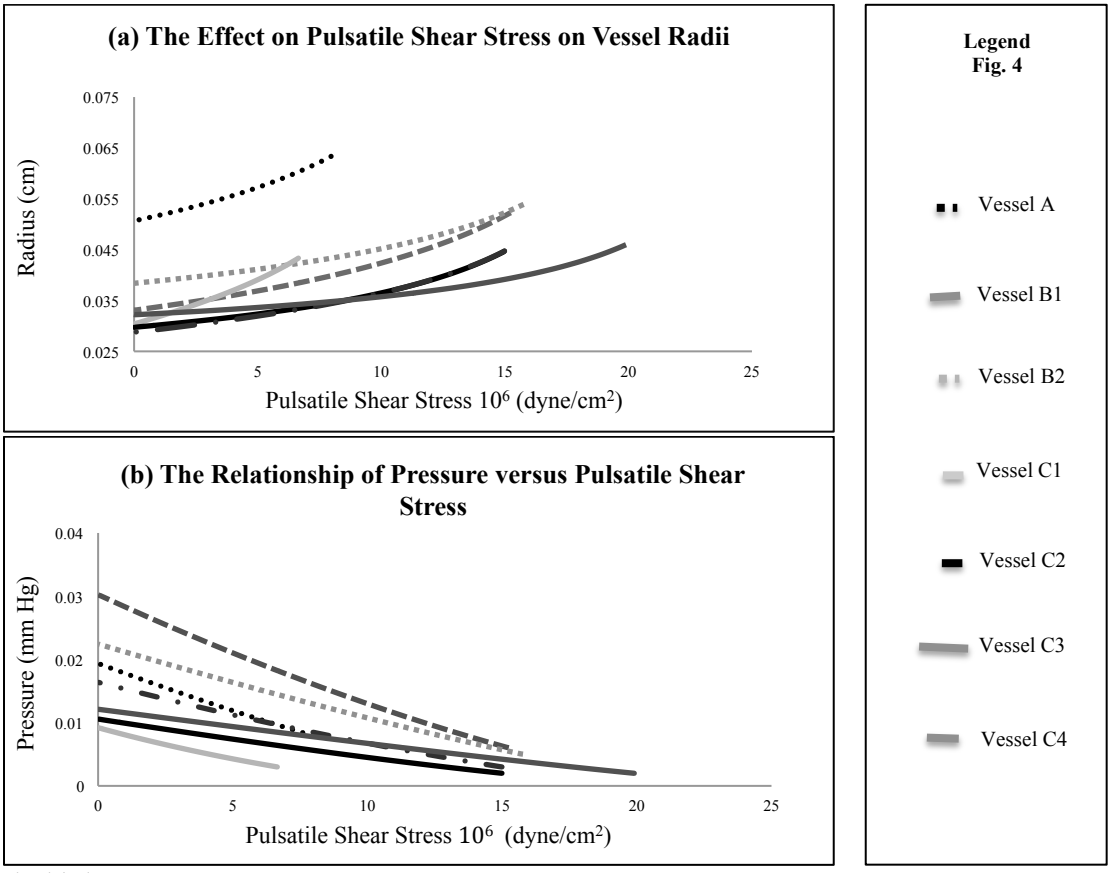

AhmedBimal©

Figure 4*. A Decrease in Pulsatile Shear Stress caused an Increase in Resistance. Graph (a) validated that a decrease in inlet pulsatile blood flow resulted in a decrease in the vascular radii and hence an increase in vascular resistance. Graph (b) demonstrated that an increase in inlet pulsatile blood flow caused a decrease in pressure and hence a decrease in vascular resistance.*

As inlet pulsatile flow was decreased, the microvessels in the network degenerated (radius shrinking until the vessel experienced minimal flow) one after the other (*Figure 5*). At 30% pulsatile shear stress, six of the vessels degenerated, with only one remaining patent. To compensate for the increased resistance, the final vessel increased in size, forming a large shunt, which is analogous to arteriovenous malformation (AVM).

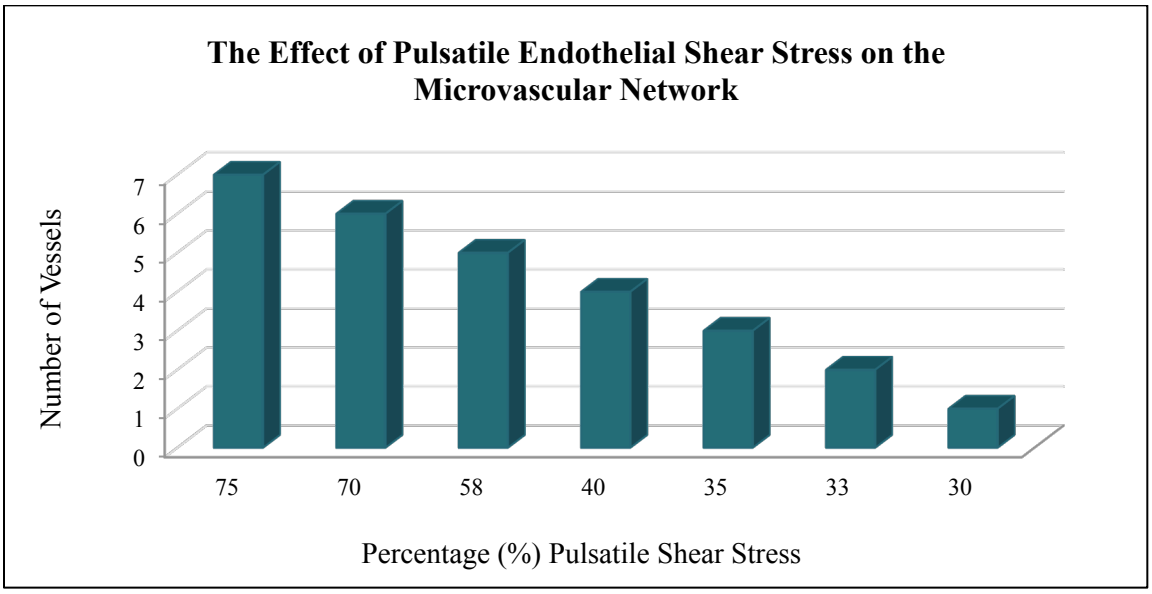

AhmedBimal©

Figure 5. *Effect of Pulsatile Shear Stress on the Microvascular Network. The graph elucidated that a decrease in the inlet pulsatile blood flow resulted in capillary rarefaction and ultimately AVM formation.*

By manipulating the pulsatility of the inlet blood flow, we studied the hemodynamic adaptation of physiological, asymmetric, and symmetric microvascular networks (*Figure 6*). A physiologically normal network (with properties as in Smaje et al. and Salotto et al.) adapted while retaining structural stability: even at 50% pulsatile blood flow (*Figure 6a (ii)*) all vessels remained viable. The asymmetric and symmetric vascular networks each ultimately had three vessels degenerate, while the normal network (*Figure 6a (iii)*) only had two vessels degenerate.

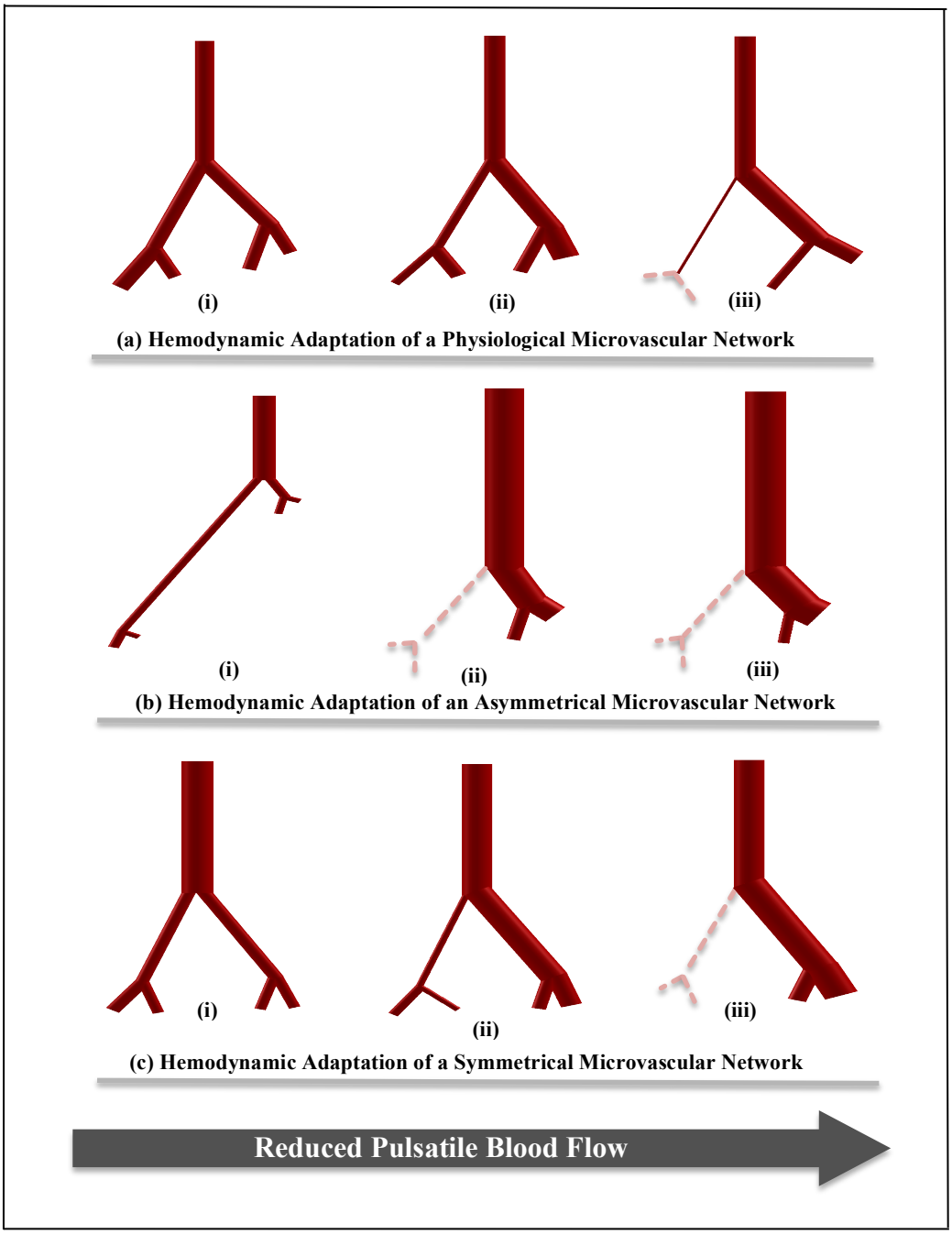

AhmedBimal©

Figure 6. *The Hemodynamic Adaptation of Different Microvascular Networks to a Pulsatile Blood Flow. As described by the figure, a normal physiological network (a) hemodynamically adapts much more efficiently than an asymmetric (b) or symmetric (c) microvascular network. This is because the rate and severity of AVM formation and capillary rarefaction is much lower in a normal microvascular structure than that of an asymmetrical or symmetrical vascular bed, (Note: (i) refers to 100 % pulsatile blood flow, (ii) refers to 50% pulsatile blood flow, and (iii) refers to 0% pulsatile blood flow.)*

By manipulating the inlet pulsatile blood flow we also studied the effect of pulsatile shear stress on vessel radii (*Figure 7*). Here again, the data shows that a physiological structure (*Figure 7a*) retains the most structural integrity while adapting to a pulsatile endothelial shear stress: even when the pulsatile blood flow is significantly reduced, four viable vessels remained. However, the asymmetric model (*Figure 7b*) led to reduced viability of the capillaries and the formation of large shunts. Meanwhile, the symmetrical model (*Figure 7c*) is not characteristic of *in vivo* behavior of microvessels: though this model adapts, all the vessels close off at once impeding blood flow into the rest of the circulatory system.

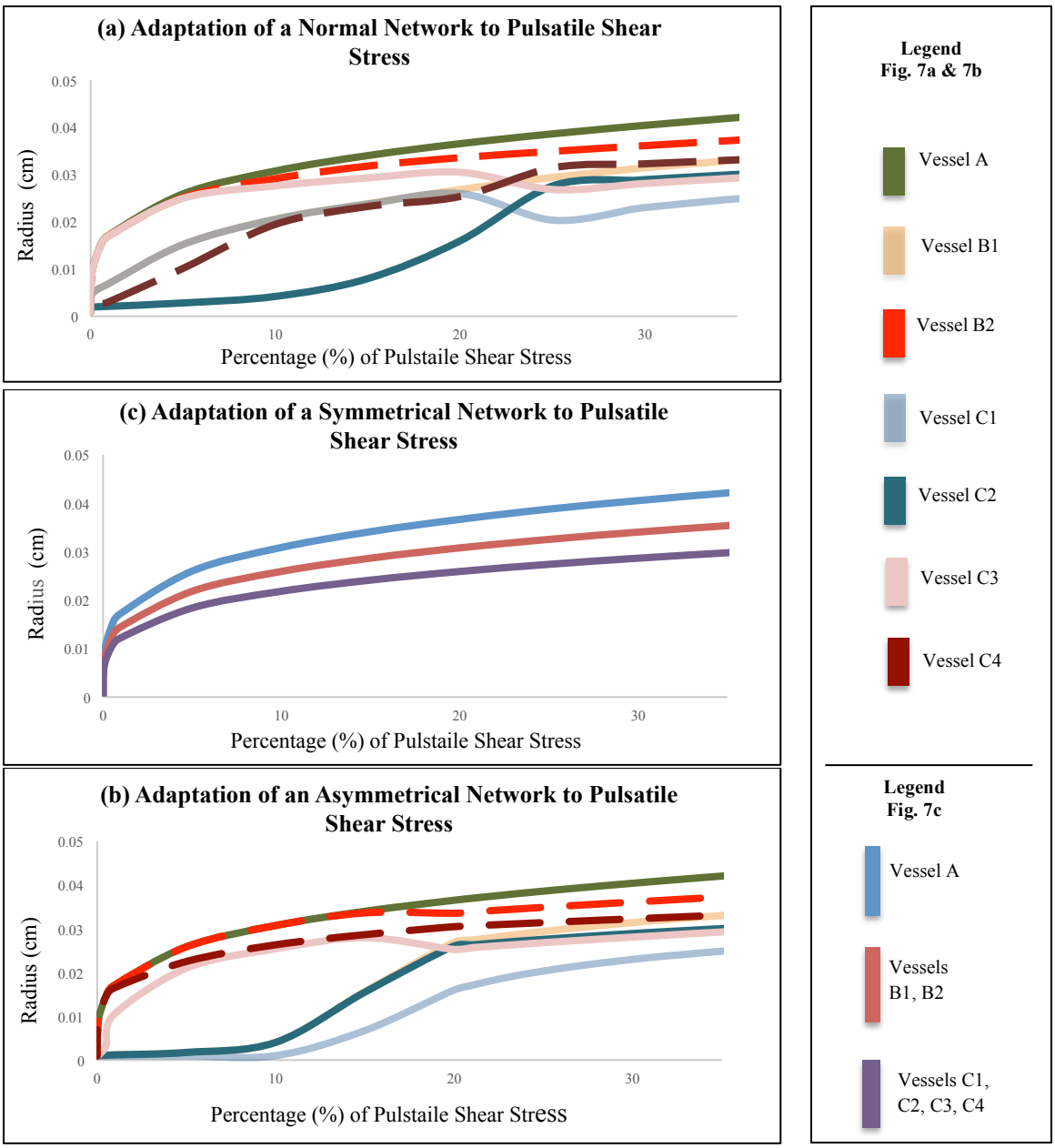

AhmedBimal©

***Figure** 7. The Adaptation of Microvascular Symmetry and Asymmetry to Pulsatile Shear Stress. In a normal vascular network (Graph (a)), at extremely low pulsatile blood flow there are four viable vessels. However, in an asymmetrical vasculature (Graph (b)) there are only two viable vessels present at a low pulsatile blood flow. A symmetric structure (Graph (c)) is not indicative of normal physiology, as all capillaries undergo rarefaction at the same rate, which provides no outlet path for blood flow. Hence, a physiological structure that is slightly asymetrical as shown in Graph (a) is preferable for normal physiologic functioning of the microvessels.*

We also analyzed how an upstream and a downstream resistance altered the response of vessels to a pulsatile shear stress. Increasing the blood flow into the microvasculature increased the upstream resistance. At extremely high upstream resistance (*Figure 8a*) the microvasculature adapted like a symmetrical structure (*Figure 7c*). Changing the terminal resistances of the vessels altered the downstream resistance. Significantly increasing the downstream resistance allowed to microvasculature to mimic the behavior of a symmetrical structure (*Figure 8b*). For downstream resistances above 0.0375 mm Hg/(ml/s), the microvessels adapt in a manner that mimics the symmetrical model (*Figure 9*).

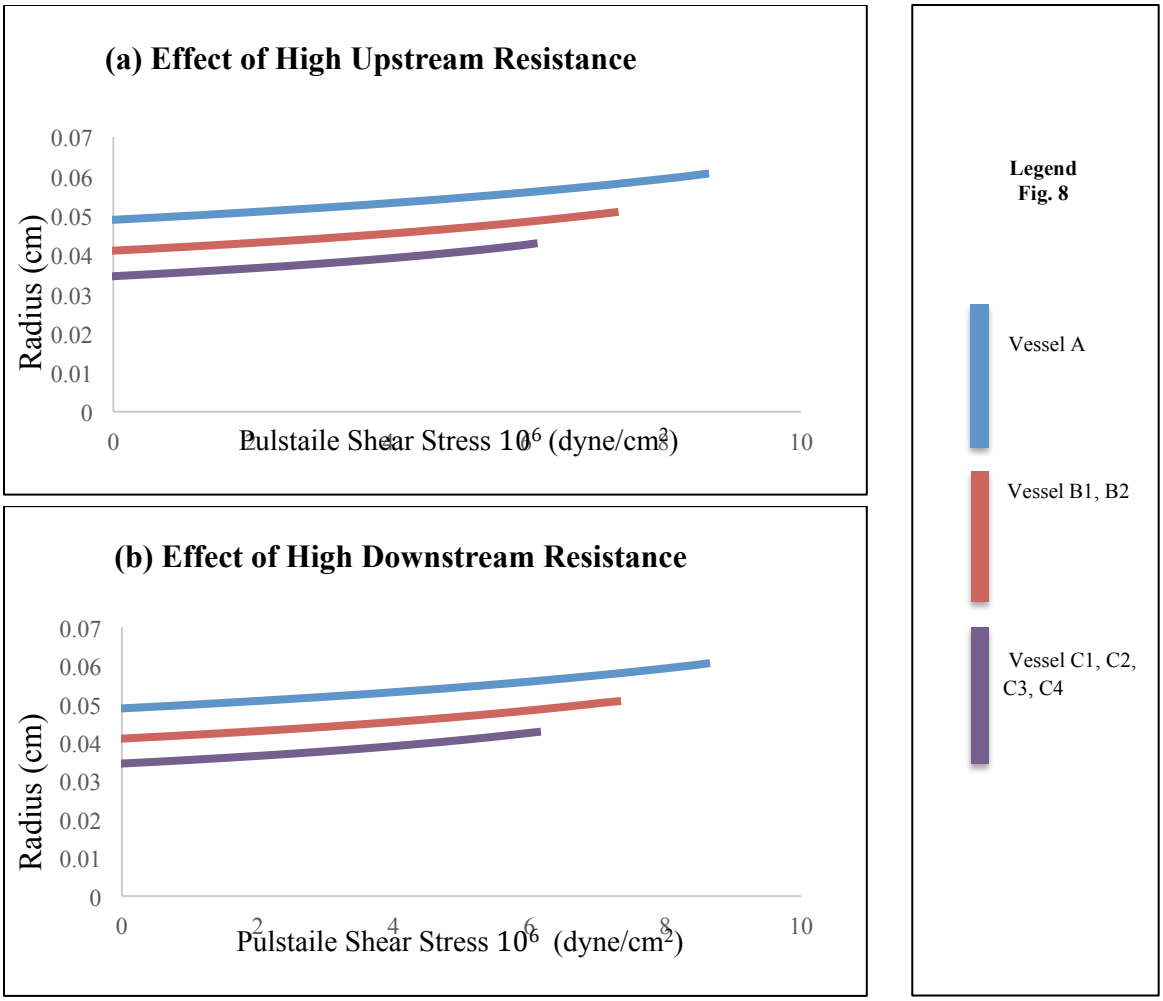

Figure 8. *The Effect of Significantly Increased Upstream and Downstream Resistance on the Radii of the Microvessels. As illustrated by these graphs a high upstream and downstream resistance resulted in the microvasculature mimicking a symmetrical non-physiological microvascular network.*

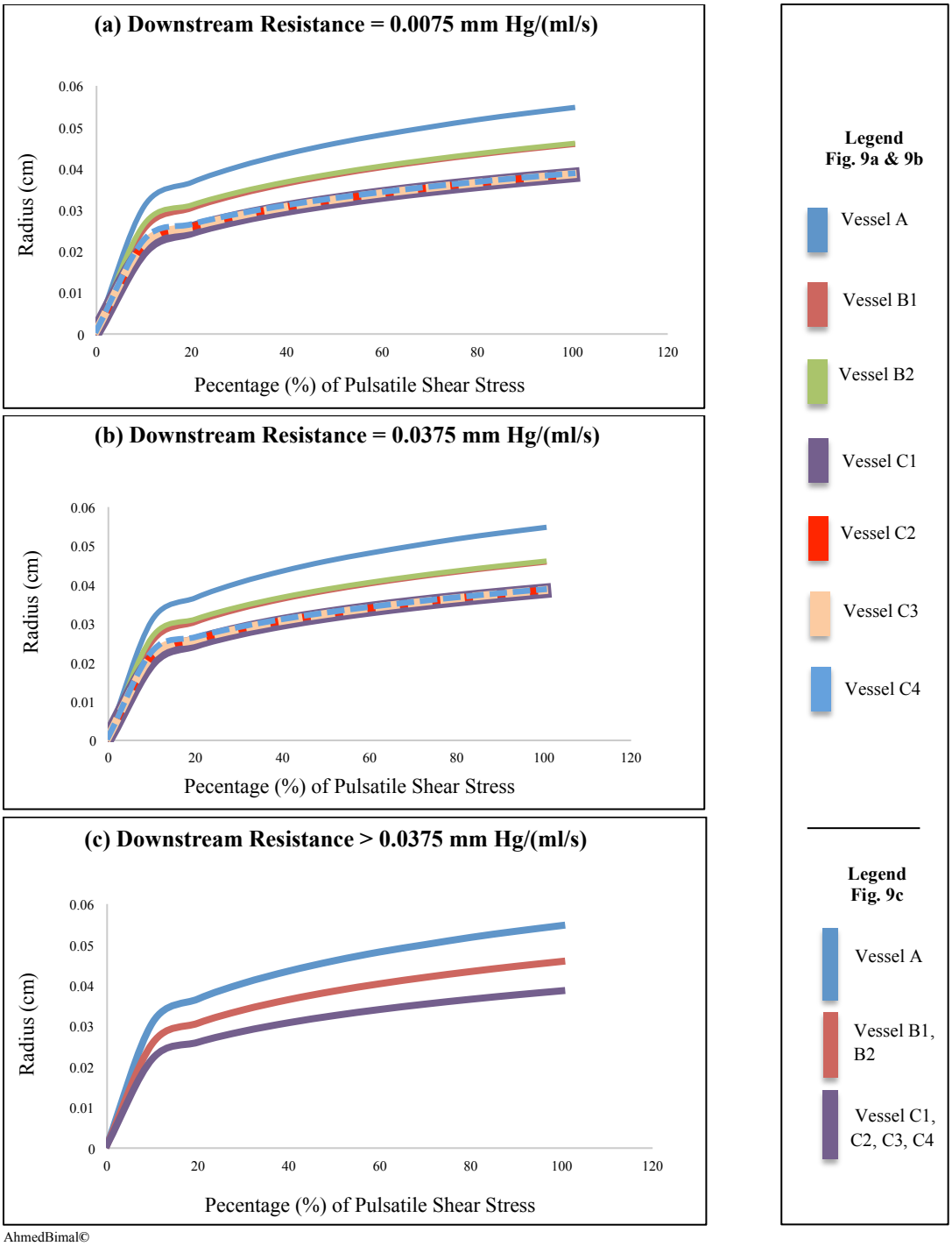

Figure 9. *The Effect of Down Stream Resistance on the radii of Microvascular Network. As indicated in these graphs, at a resistance of greater 50 Ohms produced a non-physiological response in the microvasculature.*

Each vessel is affected by the relationship between pulsatile shear stress and radius. The intersection of this relationship, the balance point, is the equilibrium shear stress and

vessel radius. A balance point curve, as shown in *Figure 10*, was constructed for each of the vessels used in our model.

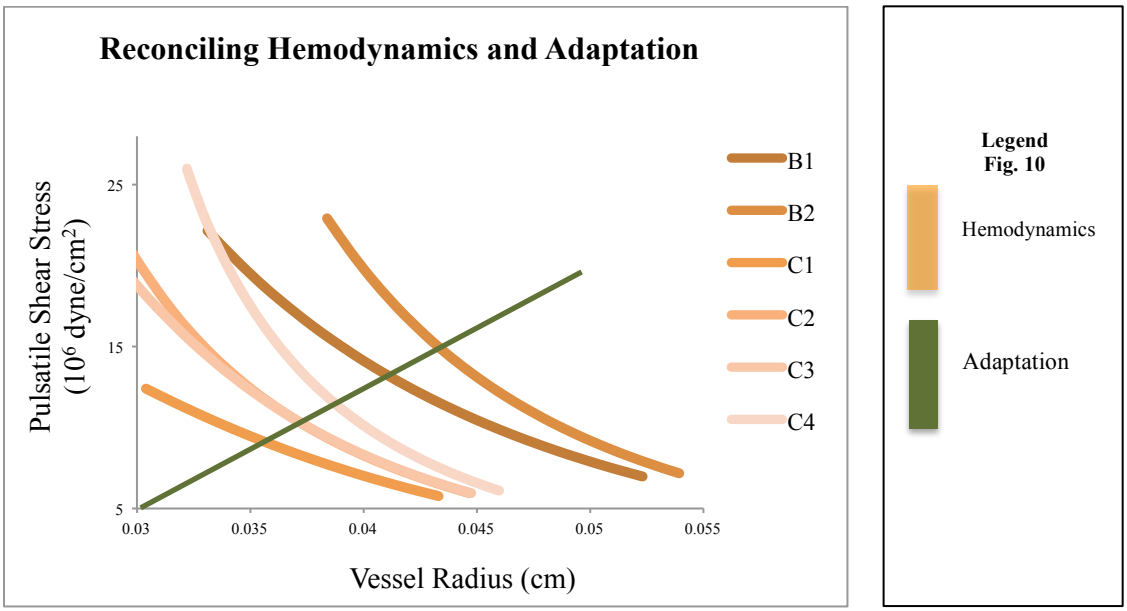

Figure 10. *Reconciling Hemodynamics (or Biomechanics) and Microvascular Adaptation (or Mechanobiology). Integrating the innate characteristics of hemodynamic and microvascular adaptation allowed us to study the mechanisms underlying vascular adaption.*

CHAPTER IV

DISCUSSION

Our work has characterized the adaptation of a model of the microvasculature in response to changes in pulsatile endothelial shear stress. An adaptive rule was identified that predicts the equilibrium state of the microvessels. The equilibrium mechanical properties, pulsatile hemodynamics, and vascular shear stresses may be predicted directly from this single adaptive rule. Even though the model used in this work was simple, it was able to characterize the complex interactions inherent to the microvasculature by combining the constitutive equations for blood pressure and flow, the mechanical stress, and commonly assumed stimuli of microvascular adaptation.

This simple model was in turn able to characterize the general adaptive trend affecting microvascular networks. By placing restrictions on the extent of our model's parameters and keeping the prescribed network as simple as possible, we did not add any additional variables to ensure structural stability. Accordingly, our results may have more generalizable application.

Due to the lack of data available on microvascular adaptation, a more conservative approach was used when modeling our network of microvessels [15]. Developing the model in this manner involved using four approaches. Firstly, the vascular stimuli were limited to the local mechanical stresses. This approached did not take into account other stimuli such as metabolites or oxygen concentration. Secondly, the stimuli of local

mechanical shear stress were limited even further to include only endothelial shear stress. This approach disregarded the effects of wall circumferential stress, torsion, and axial stress. Thirdly, we assumed that each mechanical property had only one contributing stimulus. Fourthly, we assumed that the adaptive rule was linear in order to prescribe a simple case without additional parameters. The mentioned restrictions served to pare the model down to a very simple case.

Adaptive stimuli are by no means limited to what we have modeled. It is certainly possible for the microvasculature to adapt in response to other mechanical stresses, such as wall circumferential stress or torsion. Models exploring these and other possibilities, using our methods and theoretical framework, may also guide future research.

Traditionally, the biomechanics and mechanobiology approaches have been entirely distinct from one another. Recently, though, there has been interest in integrating these fields in order to more fully understand the natural adaptive response of blood vessels. It was by combining aspects of each of these disciplines that we were able to use a balance point approach to address our initial query. This is advantageous in that it allows us to relate a specific mechanism to the complex adaptive response.

CHAPTER V

CONCLUSION

Previous clinical studies have reported an association between conditions that reduce pulsatile blood flow in the microvasculature and life-threatening comorbidities [4,17]. If the underlying mechanism for the development of these comorbidities was fully characterized, it would be possible to focus both clinical and basic research approaches. It was to this end that we became interested in the relationship between the mechanical environment of the blood vessels and their adaptive response.

Reductions in inlet pulsatile blood flow resulted in the development of behaviors very similar to reported severe morbidities [4]. Our model showed that as the pulsatile component became negligible, whole branches of the microvessels collapsed. Neighboring vessels then expanded to compensate for the significant increase in resistance due to the disappearance of the microvessels. These behaviors are analogous to the initiation of capillary rarefaction [32] and the development of arteriovenous malformations [33] reported secondary to reduced pulsatility.

In the present work, mathematical modeling provides three major benefits over experimental approaches. First, experiments alone cannot clarify the underlying mechanism that causes the development of these morbidities. Physiological systems are composed of a myriad of confounding factors that makes it difficult to infer causality from correlations. Second, living systems cannot be observed in the intermediate stages

of vascular growth and regression. Furthermore, adaptive responses cannot be halted or even controlled. Mathematical modeling provides a means to observe and control the stages of adaptation, further allowing for full characterization. Third, mathematical models significantly reduce the total number of animals needed in experimental studies without compromising the quality of the results.

REFERENCES

1. Go AS, Mozaffarian D, Roger VL, Benjamin EJ, Berry JD, Blaha MJ, Dai S, Ford ES, Fox CS, Franco S, Fullerton HJ, Gillespie C, Hailpern SM, Heit JA, Howard VJ, Huffman MD, Judd SE, Kissela BM, Kittner SJ, Lackland DT, Lichtman JH, Lisabeth LD, Mackey RH, Magid DJ, Marcus GM, Marelli A, Matchar DB, McGuire DK, Mohler ER 3rd, Moy CS, Mussolino ME, Neumar RW, Nichol G, Pandey DK, Paynter NP, Reeves MJ, Sorlie PD, Stein J, Towfighi A, Turan TN, Virani SS, Wong ND, Woo D, Turner MB; on behalf of the American Heart Association Statistics Committee and Stroke Statistics Subcommittee. Heart disease and stroke statistics—2014 update: a report from the American Heart Association. *Circulation*. 2014: published online December 18, 2013, 10.1161/01.cir.0000441139.02102.80.

2. Thoratec Corporation. Summary of Safety and Effectiveness Data. Food and Drug Adm. http://www.accessdata.fda.gov/cdrh_docs/pdf6/P060040S005b.pdf. Published Januray 20th 2010. Accessed April 3rd 2014.

3. Rose EA, Gelijns AC, Moskowitz AJ, et al. Long-term use of a left ventricular assist device for end-stage heart failure. N Engl J Med. 2001;345(20):1435-43.

4. Wever-pinzon O, Selzman CH, Drakos SG, et al. Pulsatility and the risk of nonsurgical bleeding in patients supported with the continuous-flow left ventricular assist device HeartMate II. Circ Heart Fail. 2013;6(3):517-26.

5. Givertz MM. Cardiology patient pages: ventricular assist devices: important information for patients and families. Circulation. 2011;124(12):e305-11.

6. Slaughter MS, Pagani FD, Rogers JG, et al. Clinical management of continuous-flow left ventricular assist devices in advanced heart failure. J Heart Lung Transplant. 2010;29(4 Suppl):S1-39.

7. S. Hales, *Statical Essays: Containing Haemostaticks*, vol.II. London, England: Innys and Manby; 1733.

8. Smaje LH, Fraser PA, Clough G. The dispensability of single capillaries and venules in the cat mesentery. Microvascular Res. 1980;20(3):358-70.

9. Puri N.N., Li K-J, Fich S., and Welkowitz W. Control System for Circulatory Assit Devices: Determination of Suitable Control Variables. Trans Am Soc Artif Intern Organs. 1982; XXVII: 127-132.

10. Womersley JR. Oscillatory flow in arteries: the constrained elastic tubes as a model of arterial flow and pulse transmission. Phys Med Biol. 1957;2(2):178-87.

11. Salotto AG, Muscarella LF, Melbin J, Li JK, Noordergraaf A. Pressure pulse transmission into vascular beds. Microvasc Res. 1986;32(2):152-63.

12. O'rourke MF, Cartmill TB. Influence of aortic coarctation on pulsatle hemodynamics in the proximal aorta. Circulation. 1971;44(2):281-92.

13. Milnor WR**.** *Hemodynamics*. Baltimore: Williams & Wilkins, 1989.

14. Westerhof N, Bosman F, De vries CJ, Noordergraaf A. Analog studies of the human systemic arterial tree. J Biomech. 1969;2(2):121-43.

15. Nguyen, P. H., Knezek S.F., Mohiuddin M.W., Quick C.M. The Complex Distribution of the Systemic Arterial System Mechanical Properties, Pulsatile Hemodynamics, and Vascular Stresses can Emerge from Two Simple Adaptive Rules. Unpublished manuscript, College of Veterinary Medicine, Texas A&M University College Station, TX. 2014.

16. Quick CM, Baldick HL, Safabakhsh N, et al. Unstable radii in muscular blood vessels. Am J Physiol. 1996;271(6 Pt 2):H2669-76.

17. Letsou GV, Shah N, Gregoric ID, Myers TJ, Delgado R, Frazier OH. Gastrointestinal bleeding from arteriovenous malformations in patients supported by the Jarvik 2000 axial-flow left ventricular assist device. J Heart Lung Transplant. 2005;24(1):105-9.

18. Crow S, John R, Boyle A, et al. Gastrointestinal bleeding rates in recipients of nonpulsatile and pulsatile left ventricular assist devices. J Thorac Cardiovasc Surg. 2009;137(1):208-15.

19. Demirozu ZT, Radovancevic R, Hochman LF, et al. Arteriovenous malformation and gastrointestinal bleeding in patients with the HeartMate II left ventricular assist device. J Heart Lung Transplant. 2011;30(8):849-53.

20. Cappell MS, Lebwohl O. Cessation of recurrent bleeding from gastrointestinal angiodysplasias after aortic valve replacement. Ann Intern Med. 1986;105(1):54-7.

21. Rieder MJ, Roman RJ, Greene AS. Reversal of microvascular rarefaction and reduced renal mass hypertension. Hypertension. 1997;30(1 Pt 1):120-7.

22. O'rourke MF, Cartmill TB. Influence of aortic coarctation on pulsatle hemodynamics in the proximal aorta. Circulation. 1971;44(2):281-92.

23. Tricot O, Mallat Z, Heymes C, Belmin J, Lesèche G, Tedgui A. Relation between endothelial cell apoptosis and blood flow direction in human atherosclerotic plaques. Circulation. 2000;101(21):2450-3.

24. Travis AR, Giridharan GA, Pantalos GM, et al. Vascular pulsatility in patients with a pulsatile- or continuous-flow ventricular assist device. J Thorac Cardiovasc Surg. 2007;133(2):517-24.

25. Hudlicka O, Brown MD. Adaptation of skeletal muscle microvasculature to increased or decreased blood flow: role of shear stress, nitric oxide and vascular endothelial growth factor. J Vasc Res. 2009;46(5):504-12.

26. Pries AR, Secomb TW, Gaehtgens P. Structural adaptation and stability of microvascular networks: theory and simulations. Am J Physiol. 1998;275(2 Pt 2):H349-60.

27. Fry BC, Roy TK, Secomb TW. Capillary recruitment in a theoretical model for blood flow regulation in heterogeneous microvessel networks. Physiol Rep. 2013;1(3):e00050.

28. Wiederhielm CA, Woodbury JW, Kirk S, Rushmer RF. Pulsatile Pressures in the Microcirculation of Frog's Mesentery. Am J Physiol. 1964;207:173-6.

29. Vawter D, Fung YC, Zweifach BW. Distribution of blood flow and pressure from a microvessel into a branch. Microvascular Res. 1974;8(1):44-52.

30. Intaglietta M, Pawula RF, Tompkins WR. Pressure measurements in the mammalian microvasculature. Microvascular Res. 1970;2(2):212-20.

31. Greenberg JH, Reivich M, Noordergraaf A. A model of cerebral blood flow control in hypercapnia. Ann Biomed Eng. 1978;6(4):453-91.

32. Serné EH, Gans RO, Ter maaten JC, Tangelder GJ, Donker AJ, Stehouwer CD. Impaired skin capillary recruitment in essential hypertension is caused by both functional and structural capillary rarefaction. Hypertension. 2001;38(2):238-42.

33. Mccormick WF. The pathology of vascular ("arteriovenous") malformations. J Neurosurg. 1966;24(4):807-16.

APPENDIX A

WESTERHOFF MODEL NETWORK

```
% Westerhoff code created by Phuc Nguyen, altered to work for a simple
microvascular model by Sara Ahmed

% VESSEL LENGTHS

% % Salotto, et al

lA=.04;
lB1=0.03;
lB2=0.025;
lC1=0.001;
lC2=0.0015;
lC3=0.001;
lC4=0.0015;

% RADII

% salotto values *10^2*2 and levels made different
rA=.05*2*2;
rB1=.04*2;
rB2=.035*2;
rC1=.0031*2;
rC2=.027*2;
rC3=.031*2;
rC4=.0027*2;

% WALL THICKNESSES

% salotto values
hA=45e-6;
hB1=12e-6;
hB2=10e-6;
hC1=8e-6;
hC2=6e-6;
hC3=8e-6;
hC4=6e-6;

% YOUNG'S MODULI
% ___*10^6

% salotto values
EA=16e6;
EB1=18e6;
EB2=19e6;
EC1=20e6;
EC2=21e6;
EC3=20e6;
EC4=21e6;
```

```
% TERMINAL RESISTANCES
% Westerhof's original reistances 1 Ohm = 1 g/(sec*cm^4)
R1 = 1;
R2 = 1;
R3 = 1;
R4 = 1;


% PUT IN NETWORK MATRIX
% MAP OF THE MODEL

% INPUT INTO PARAMETERS VESSEL PARAMETER MATRIX
%+++++++++++++++++++++++++++++++++++++++++++++++++++++++++++++++++++++++
++++

V(1,:) = [1 2 rA  EA  lA  hA  0 0]; %top vessel
V(2,:) = [2 3 rB1 EB1 lB1 hB1 0 0]; %mid left
V(3,:) = [2 4 rB2 EB2 lB2 hB2 0 0]; %mid right
V(4,:) = [3 5 rC1 EC1 lC1 hC1 0 0]; %botton left
V(5,:) = [3 6 rC2 EC2 lC2 hC2 0 0]; %botton 2nd left
V(6,:) = [4 7 rC3 EC3 lC3 hC3 0 0]; %bottom 2nd right
V(7,:) = [4 8 rC4 EC4 lC4 hC4 0 0]; %bottom right


% TERMINAL RESISTANCES
%+++++++++++++++++++++++++++++++++++++++++++++++++++++++++++++++++++++++
++++
%v(XXX,1) = VESSEL NUMBER
%V(XXX,2) = NODAL NUMBER

V(8,:)  = [5 5 0 0 0 0 R1 1];
V(9,:)  = [6 6 0 0 0 0 R2 1];
V(10,:) = [7 7 0 0 0 0 R3 1];
V(11,:) = [8 8 0 0 0 0 R4 1];


RTT(1) = R1;
RTT(2) = R2;
RTT(3) = R3;
RTT(4) = R4;


% Original Westerhof Values
OE = V(1:7,4); Or = V(1:7,3); Oh = V(1:7,6); l = V(1:7,5); RT =
V(8:11,7);
```

APPENDIX B

WESTERHOFF MODEL

```
function [Pt Qt RCL] = WM(ri, Ei, Ri, li, hi, Qi, HR, r, E, h, l, RT,
V, Qin)

Qin = Qin*Qi;
FQin = fft(Qin);
%++++++++++++++++++++++++++++++++++++++++++++++++++++++++++++++++++++
++++
cc = 10;
% Cut-off harmonic to filter out high frequency
%++++++++++++++++++++++++++++++++++++++++++++++++++++++++++++++++++++
++++

V(1:7,3) = r';
V(1:7,4) = E';
V(1:7,5) = l';
V(1:7,6) = h';
V(8:11,7) = RT;

% GLOBAL PARAMETERS
%++++++++++++++++++++++++++++++++++++++++++++++++++++++++++++++++++++
++++
mu = 0.03;
% Dynamic viscosity of blood
rho = 1.050;
% Blood density
%--------------------------------------------------------------------
----



% Convsersion factors
Ei = Ei*10^6;
% Elastic factor, default is 10^6
Ri = Ri*1000;
% Terminal resistance factor, default is 1000

for k = 1:length(V(:,1))
    if V(k,8) == 0
        V(k,3) = V(k,3)*ri;
        V(k,4) = V(k,4)*Ei;
        V(k,5) = V(k,5)*li;
        V(k,6) = V(k,6)*hi;
    else
        V(k,7) = V(k,7)*Ri;
    end
end
%--------------------------------------------------------------------
----
```

```
% CALCULATE PRESSURES AND FLOW
%+++++++++++++++++++++++++++++++++++++++++++++++++++++++++++++++++++++++++
++++
f = HR/60;
gnd = max(V(:,2)) + 1;
Qin = zeros(gnd,1);
for n = 1:length(FQin(2:length(FQin)))/2 + 1

    % CALCULATE THE VESSEL IMPEDANCE

%+++++++++++++++++++++++++++++++++++++++++++++++++++++++++++++++++++++++++
    w = (n-1)*2*pi*f;
    N = length(V(:,1));

    for k = 1:N
        if V(k,8) == 0
            iM(k,1) = V(k,1); iM(k,2) = V(k,2);
            r = V(k,3); E = V(k,4); l = V(k,5); h = V(k,6);

            C = ((3*pi*(r^2).*((r + h).^2))/(E.*h.*(2*r + h)))*l;
            L = (rho/(pi*(r^2)))*l;
            R = (8*mu*l)/(pi*(r^4));

            RCL(k,1) = R; RCL(k,2) = C; RCL(k,3) = L;

            iM(k,3) = R + i*w*L;
            iM(k,4) = 1/(i*w*C);

            iM(k,5) = V(k,7); iM(k,6) = V(k,8);
        else
            iM(k,1) = V(k,1); iM(k,2) = V(k,2);
            iM(k,5) = V(k,7); iM(k,6) = V(k,8);
        end

    end
    %-------------------------------------------------------------------
----

    % CALCULATE THE CONDUCTANCE MATRIX

%+++++++++++++++++++++++++++++++++++++++++++++++++++++++++++++++++++++++++
    C = zeros(gnd,gnd);
    IM = iM;
    for k = 1:N
        if IM(k,6) == 0
            C(IM(k,1),IM(k,2)) = C(IM(k,1),IM(k,2)) - 1/IM(k,3);
            C(IM(k,2),IM(k,1)) = C(IM(k,1),IM(k,2));
            C(IM(k,1),gnd) = C(IM(k,1),gnd) - 1/IM(k,4);
            C(IM(k,1),IM(k,1)) = C(IM(k,1),IM(k,1)) + 1/IM(k,3) +
1/IM(k,4);
            C(IM(k,2),IM(k,2)) = C(IM(k,2),IM(k,2)) + 1/IM(k,3);
            C(gnd,gnd) = C(gnd,gnd) + 1/IM(k,4);
        else
            C(IM(k,2),gnd) = C(IM(k,2),gnd) - 1/IM(k,5);
            C(IM(k,2),IM(k,2)) = C(IM(k,2),IM(k,2)) + 1/IM(k,5);
```

```
            C(gnd,gnd) = C(gnd,gnd) + 1/IM(k,5);
        end
    end
    %-------------------------------------------------------------------
----

    Qin(1) = FQin(n);

    Pn = C\Qin;
    P(:,n) = Pn;
    for l = 1:length(IM(:,1))
        if IM(l,6) == 0
            Qn(l) = (Pn(IM(l,1)) - Pn(IM(l,2)))/IM(l,3);
        else
            Qn(l) = (Pn(IM(l,2)) - Pn(gnd))/IM(l,5);
        end
    end
    Q(:,n) = Qn;
end

% CALCULATE PRESSURES AND FLOWS
%+++++++++++++++++++++++++++++++++++++++++++++++++++++++++++++++++++++++
x = length(FQin);
px = length(FQin(2:x))/2 + 1;

mk = px + 1;
k = 0;
while mk < length(FQin)
    fk = 2*k + 1;
    k = k + 1;
    mk = px + k;
    P(:,mk) = real(P(:,mk-fk)) - i*imag(P(:,mk-fk));
    Q(:,mk) = real(Q(:,mk-fk)) - i*imag(Q(:,mk-fk));
end


% filtering the signal
c = length(P(1,:))-cc;
for k = 1:length(P(:,1))
    P(k,cc+2:c) = 0;
    Q(k,cc+2:c) = 0;
end


% reconstructing the signal
for k = 1:length(Q(:,1))
    Qt(k,:) = ifft(Q(k,:));
end

% reconstructing the signal
for k = 1:length(P(:,1))
    Pt(k,:) = ifft(P(k,:));
end
%-------------------------------------------------------------------
----
```

APPENDIX C

INPUT PULSATILE BLOOD FLOW (SaraTiaLVAD)

```
% THIS CODE PERFORM TEST ON ALL ADAPTIVE FUNCTIONS FOR THE GIVEN
PARAMETERS
%++++++++++++++++++++++++++++++++++++++++++++++++++++++++++++++++++++++
++++
clear; clc;
close all;


% PERTURBATION PARAMETERS
%++++++++++++++++++++++++++++++++++++++++++++++++++++++++++++++++++++++
++++
ri = 1;     hi = 1;     Ei = 1/1.5;

Qi = 1.2;               % MODIFY INPUT FLOW RATE
Ri = 1/1.2;             % MODIFY TOTAL PERIPHERAL RESISTANCE
HI = 1.0;               % MODIFY HEART RATE
li = 1;                 % MODIFY VESSEL LENGTHS
%----------------------------------------------------------------------
----


% SET NETWORK AND BOUNDARY CONDITIONS
%++++++++++++++++++++++++++++++++++++++++++++++++++++++++++++++++++++++
++++
run WMN; run AorticFlow;
%----------------------------------------------------------------------
----
HR = 70*HI;             % HEART RATE
%----------------------------------------------------------------------
----
%----------------------------------------------------------------------
----
%----------------------------------------------------------------------
----
%----------------------------------------------------------------------
----


% SIMULATION LVAD IMPLANTATION
%++++++++++++++++++++++++++++++++++++++++++++++++++++++++++++++++++++++
++++
LVADStrength = 25;

%----------------------------------------------------------------------
----
% Modify flow amplitude

Qin = Qi*Qin;
```

```
% Modify flow for LVAD
%-------------------------------------------------------------------------
----
FQin = fft(Qin);
a = length(FQin);
MFQin(1) = FQin(1);
MFQin(2:a) = ((100 - LVADStrength)/100)*FQin(2:a);
MQin = ifft(MFQin);
% %-----------------------------------------------------------------------
------
% figure; plot(t, MQin); title('Combined LVAD and Heart Flow');
% ylabel('Flow Rate (mL)'); xlabel('Time');
% %-----------------------------------------------------------------------
------



%+++++++++++++++++++++++++++++++++++++++++++++++++++++++++++++++++++++++++
++++
g = 0.1; SI = 0.0001;
%-------------------------------------------------------------------------
----
rops = 0.0009;          % Tia Bimal's value for small vessels
kSps = 0.000834;         % ESTIMATED USING GRADIENT DESCENT

% ESTABLISH BASELINE TO PREDICT COLLATERAL IN NORMAL CONDITION
%-------------------------------------------------------------------------
----
[Pt Qt RCL r] = AdaptRadiusPulseShear(rops, kSps, HR, V, SI, g, Qin,
Qi, ri, Ei, Ri, li, hi);
% [Pt Qt RCL r] = AdaptRadiusMeanShear(rops, kSps, HR, V, SI, g, Qin,
Qi, ri, Ei, Ri, li, hi);
%-------------------------------------------------------------------------
----


% REMODELING TO REDUCED PULSATILITY
%-------------------------------------------------------------------------
----
[LVADPt LVADQt LVADRCL LVADr] = AdaptRadiusPulseShear(rops, kSps, HR,
V, SI, g, MQin, Qi, ri, Ei, Ri, li, hi);
% [LVADPt LVADQt LVADRCL LVADr] = AdaptRadiusMeanShear(rops, kSps, HR,
V, SI, g, MQin, Qi, ri, Ei, Ri, li, hi);
%-------------------------------------------------------------------------
----


% PLOT VESSELS
rr(1,:) = r(1:7);
rr(2,:) = LVADr(1:7);
%
% figure; bar(rr'); legend('Original','Adapted');
% ylabel('Vessel Radius (cm)'); xlabel('Vessel Number');
```

APPENDIX D

PERTURBATION ANALYSIS

```
% THIS CODE PERFORM TEST ON ALL ADAPTIVE FUNCTIONS FOR THE GIVEN
PARAMETERS
%++++++++++++++++++++++++++++++++++++++++++++++++++++++++++++++++++++++
++++
clear; clc;
close all;


% PERTURBATION PARAMETERS
%++++++++++++++++++++++++++++++++++++++++++++++++++++++++++++++++++++++
++++
ri = 1;     hi = 1;     Ei = 1/1.5;

Qi = 1.2;               % MODIFY INPU FLOW RATE
Ri = 1/1.2;             % MODIFY TOTAL PERIPHERAL RESISTANCE
HI = 1.0;               % MODIFY HEART RATE
li = 1;                 % MODIFY VESSEL LENGTHS
%----------------------------------------------------------------------
----


% SET NETWORK AND BOUNDARYCONDITIONS
%++++++++++++++++++++++++++++++++++++++++++++++++++++++++++++++++++++++
++++
run WMN; run AorticFlow;
%----------------------------------------------------------------------
----
HR = 70*HI;             % HEART RATE
%----------------------------------------------------------------------
----
%----------------------------------------------------------------------
----
%----------------------------------------------------------------------
----
%----------------------------------------------------------------------
----



% ADAPTATION OF RADIUS TO PULSATILE ENDOTHELIAL SHEAR STRESS
%++++++++++++++++++++++++++++++++++++++++++++++++++++++++++++++++++++++
++++
g = 0.1; SI = 0.0001;
%----------------------------------------------------------------------
----
rops = 0.0907;
kSps = 0.001668;         % ESTIMATED USING GRADIENT DESCENT
%----------------------------------------------------------------------
```

```
----
[rpsPt rpsQt rpsRCL rpsr rpsEr] = AdaptRadiusPulseShear(rops, kSps, HR,
V, SI, g, Qin, Qi, ri, Ei, Ri, li, hi);
%-------------------------------------------------------------------
----
rpsrr(:,1) = Or; rpsrr(:,2) = rpsr;
figure;
subplot(2,1,1); bar(rpsrr);
    legend('Original','Predicted'); title('Adaptation of Radius to
Pulsatile Shear Stress');
    ylabel('Vessel Radius (cm)'); xlabel('Vessel Number');
subplot(2,1,2); plot(Or, Or,'*b'); hold on; plot(Or, rpsr,'or');
    legend('Original','Predicted');
    ylabel('Vessel Radius (cm)'); xlabel('Original Westerhof Radius
(cm)');
%-------------------------------------------------------------------
----

% % ADAPTATION OF RADIUS TO PULSATILE ENDOTHELIAL SHEAR STRESS
%
%+++++++++++++++++++++++++++++++++++++++++++++++++++++++++++++++++++
++++
% g = 0.0001; SI = 0.0001;
% %-----------------------------------------------------------------
------
% rops = 0.0907;
% kSps = 0.001668;         % ESTIMATED USING GRADIENT DESCENT
% %-----------------------------------------------------------------
------
% [rpsPt rpsQt rpsRCL rpsr rpsEr] = AdaptRadiusPulseShear(rops, kSps,
HR, V, SI, g, Qin, Qi, ri, Ei, Ri, li, hi);
% %-----------------------------------------------------------------
------
% rpsrr(:,1) = Or; rpsrr(:,2) = rpsr;
% figure;
% subplot(2,1,1); bar(rpsrr);
%     legend('Original','Predicted'); title('Adaptation of Radius to
Pulsatile Shear Stress');
%     ylabel('Vessel Radius (cm)'); xlabel('Vessel Number');
% subplot(2,1,2); plot(Or, Or,'*b'); hold on; plot(Or, rpsr,'or');
%     legend('Original','Predicted');
%     ylabel('Vessel Radius (cm)'); xlabel('Original Westerhof Radius
(cm)');
% %-----------------------------------------------------------------
------
```

APPENDIX E

AORTIC FLOW (INPUT FLOW INTO MICROVASCULATURE)

```
% TIME AND FLOW WAVEFORM OF A 28 YEAR-OLD HEALTHY MAN
t = [0
0.01
0.02
0.03
0.04
0.05
0.06
0.07
0.08
0.09
0.1
0.11
0.12
0.13
0.14
0.15
0.16
0.17
0.18
0.19
0.2
0.21
0.22
0.23
0.24
0.25
0.26
0.27
0.28
0.29
0.3
0.31
0.32
0.33
0.34
0.35
0.36
0.37
0.38
0.39
0.4
0.41
0.42
0.43
0.44
0.45
0.46
0.47
0.48
```

```
0.49
0.5
0.51
0.52
0.53
0.54
0.55
0.56
0.57
0.58
0.59
0.6
0.61
0.62
0.63
0.64
0.65
0.66
0.67
0.68
0.69
0.7
0.71
0.72
0.73
0.74
0.75
0.76
0.77
0.78
0.79
0.8
0.81
0.82
0.83
0.84
0.85
0.86
0.87
0.88
0.89
0.9
0.91
0.92
0.93
0.94
0.95
0.96
0.97
0.98
0.99
1];

Qin = [0
8.740555556
28.15
95.39444444
134.3394444
```

212.8711111
257.6783333
294.9877778
310.4355556
334.6894444
349.9055556
357.6138889
358.8733333
355.2255556
347.4883333
340.3094444
331.0477778
315.3772222
298.2283333
287.8683333
276.9022222
269.2966667
257.6338889
248.6255556
237.4488889
226.3416667
212.1716667
195.0483333
170.57
149.0194444
130.7161111
112.7455556
87.41388889
69.04611111
35.12722222
-0.705
-31.36277778
-26.09944444
-15.95777778
-7.062777778
0.539444444
5.643333333
10.40722222
14.41333333
18.515
21.68944444
22.82111111
22.42444444
20.71944444
15.94222222
10.83
7.142777778
5.271666667
3.455
1.817777778
0.877777778
0
0
0
0
0
0
0

```
0
0
0
0
0
0
0
0
0
0
0
0
0
0
0
0
0
0
0
0
0
0
0
0
0
0
0
0
0
0
0
0
0
0
0
0
0
0];


% Pressure data
Pin = [75.01
74.938
74.828
74.727
74.629
74.537
74.383
74.243
74.084
73.839
73.714
73.663
74.138
74.814
80.745
85.469
88.902
```

91.663
94.312
96.248
97.854
99.648
100.3
101.17
101.77
102.5
103.12
103.77
104.36
104.9
105.54
105.98
106.14
106.48
106.44
106.27
106.13
106.05
105.98
105.87
105.7
105.4
104.93
104.32
103.79
103.44
102.83
101.96
101.15
101.06
101.34
102.15
102.66
102.6
102.18
101.77
100.91
99.795
99.074
98.629
99.476
100.02
99.865
99.388
98.523
97.928
97.206
96.424
95.665
95.122
94.402
93.812
93.317
92.599
92.492

```
91.64
91.146
90.43
90.006
89.778
89.174
88.5
87.951
87.501
87.415
87.002
86.74
86.373
86.274
85.828
85.453
85.163
84.633
84.24
83.816
83.54
83.107
82.556
82.373
81.856
81.371
80.914
80.616
80.247
79.958
79.917
79.661
79.428
79.04
78.618
77.98
77.479
77.115
76.757
76.385
76.116
75.92
75.729
75.558
75.357
75.077
74.846
74.728
74.619
74.536
74.465
74.424
74.41];

% Convert aortic flow to micro
Qin = 0.00050026536.*Qin;
% Qin = 0.*Qin;
```

```
% Convert aortic pressure to micro
Pin = .13325.*Pin;
% Pin = 0.*Pin;
```

APPENDIX F

ADAPTATION OF RADII TO PULSATILE ENDOTHELIAL SHEAR STRESS

```
function [Pt Qt RCL r Er] = AdaptRadiusPulseShear(ro, kS, HR, V, SI, g,
Qin, Qi, ri, Ei, Ri, li, hi)
mu = 0.03;

Or = V(1:7,3); OE = V(1:7,4); Or = V(1:7,3); Oh = V(1:7,6);
RT = V(8:11,7); l = V(1:7,5);


r = ones(length(Or),1); r1 = 0; Err = 1;
while Err > SI
    rp = r;
    [Pt Qt RCL] = WM(ri, Ei, Ri, li, hi, Qi, HR, r, OE, Oh, l, RT, V,
Qin);


    Qt = Qt(1:7,:);
    for n = 1:length(Qt(:,1));
        sQ(n) = range(Qt(n,:));
    end
    mSS = (4.*mu.*sQ')./(pi.*r.^3);
%     rmsS = rms(mSS,1);

    %ro = 0.01;
    Ar = (ro + kS*mSS); Ar = r1 + (Ar - r1)*g; r1 = Ar; r = Ar;



    clc; Err = 100*sum(((r - rp)./rp).^2)/length(rp)
    MeanRadiusPulseShear = mean(r)
end

itm = 1:1:7; Er = 0;
for n = 1:length(itm);
    Er = Er + ((r(itm(n)) - Or(itm(n)))/(Or(itm(n))))^2;
end
Er = 100*Er/length(itm);
End
```

APPENDIX G

ADAPTATION OF RADII TO MEAN ENDOTHELIAL SHEAR STRESS

```
function [Pt Qt RCL r Er] = AdaptRadiusMeanShear(ro, kS, HR, V, SI, g,
Qin, Qi, ri, Ei, Ri, li, hi)
mu = 0.03;

Or = V(1:7,3); OE = V(1:7,4); Or = V(1:7,3); Oh = V(1:7,6);
RT = V(8:11,7); l = V(1:7,5);

r = ones(7,1); r1 = 0; Err = 1;
while Err > SI
    rp = r;
    [Pt Qt RCL] = WM(ri, Ei, Ri, li, hi, Qi, HR, r, OE, Oh, l, RT, V,
Qin);


    Qt = Qt(1:7,:);
    for n = 1:length(Qt(:,1));
        sQ(n) = mean(Qt(n,:));
    end
    mSS = (4.*mu.*sQ')./(pi.*r.^3);

    ro = 0.01;
    Ar = (ro + kS*mSS); Ar = r1 + (Ar - r1)*g; r1 = Ar; r = Ar;

    clc; Err = 100*sum(((r - rp)./rp).^2)/length(rp)
    MeanRadiusMeanShear = mean(r)
end

itm = 1:1:7; Er = 0;
for n = 1:length(itm);
    Er = Er + ((r(itm(n)) - Or(itm(n)))/(Or(itm(n))))^2;
end
Er = 100*Er/length(itm);
end
```

CONTACTS

Name: Sara K. Ahmed

Email Address: ahmedsara182@gmail.com

Education: Bachelor of Science in Biomedical Engineering, May 2015

Texas A&M University

Undergraduate Research Scholar 2014

Name: Tia Bimal

Email Address: tia_bimal@hotmail.com

Education: Bachelor of Science in Biomedical Sciences, August 2014

Texas A&M University

Undergraduate Research Scholar 2014

Contact Address: c/o Dr. Christopher M. Quick

Associate Professor of Physiology and Pharmacology

College of Veterinary Medicine

Texas A&M University

College Station, TX, 77840